ON DEVELOPMENT OF TOTALLY IMPLANTABLE VESTIBULAR PROSTHESIS

Andrei M. Shkel [1]

Department of Mechanical and Aerospace Engineering
4208 Engineering Gateway Building
University of California - Irvine
Irvine, California, USA, 92697
(949) 824-3843 (phone), ashkel@uci.edu

Abstract: This paper presents a functional architecture, system level design, and preliminary experimental evaluation of a unilateral vestibular prosthesis. The sensing element of the prosthesis is a custom designed one-axis MEMS gyroscope. Similarly to the natural semicircular canal, the microscopic gyroscope senses angular motion of the head and generates voltages proportional to the corresponding angular accelerations. Then, voltages are sent to the pulse generating unit where angular motion is translated into voltage pulses. The voltage pulses are converted into current pulses and are delivered through specially designed electrodes, conditioned to stimulate the corresponding vestibular nerve branch. Our preliminary experimental evaluations of the prosthesis on a rate table indicate that the device's output matches the average firing rate of vestibular neurons to those in animal models reported in the literature. The proposed design is scalable; the sensing unit, pulse generator, and the current source can be potentially implemented on a single chip using integrated MEMS technology.

Keywords: MEMS, Vestibular Prosthesis, Inertial Sensors, biosystems

1. INTRODUCTION

Sensory prostheses to artificially replace lost sensory function for a number of sensory systems are currently under investigation. For example, cochlear implants use electrical stimulation to restore hearing and provide some relief for patients suffering profound sensorineural hearing loss S.U. Ay, F.-G. Zeng, and Shen (1997). Using similar principles, a vestibular prosthesis could provide head orientation information to the nervous system for patients suffering from peripheral vestibular disorders.

The vestibular organ of the inner ear is the major anatomical system to sense motion. The primary function of the vestibular system is to provide information to the brain about the body's motion and orientation. It measures six quantities concerning the spatial orientation including 3-axes angular acceleration and 3-axes linear acceleration. Diminished balance ability, often seen in older adults, poses a serious health risk due to the increased likelihood of the falling.

Our goal is to develop an implantable, vestibular neural prosthesis using electrical stimulation. It offers potential opportunity to restore seriously diminished vestibular systems. The long term goal of this research is to explore opportunities for development of a totally implantable MEMS-based

[1] Supported by the NSF CAREER CMS-0449442

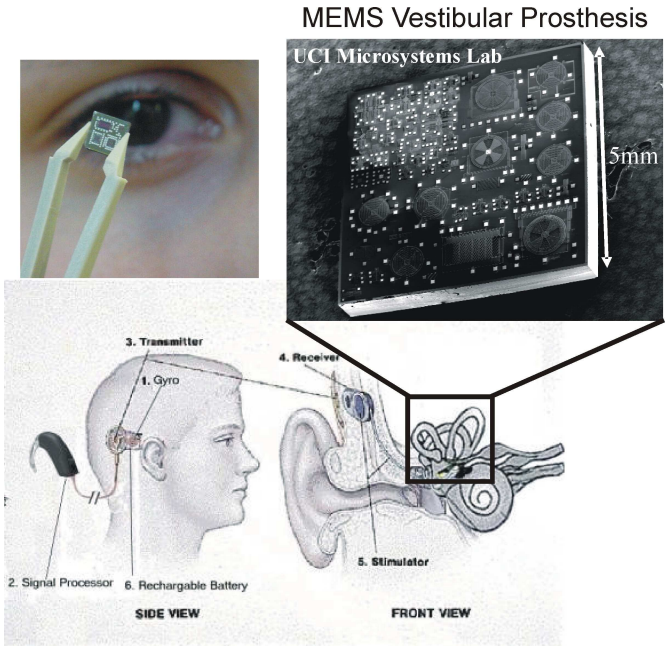

Fig. 1. A conceptual model of a totally implantable vestibular prosthesis. The implant is based on 3-axes micro-size gyroscopes integrated alongside with signal conditioning electronics on the same silicon chip

electronic device which functions identically to the vestibular system, Figure 1. Using unique feature of the MEMS technology and Integrated Circuit (IC) technology, micromachining can shrink the sensors size by orders of magnitude, reduce the fabrication cost significantly, and allow the electronics to be integrated on the same silicon chip. Figure 1 shows a 5 by 5 millimeter silicon chip developed by UCI's Micro-system lab. The chip includes prototypes of 6 gyroscopes and several linear and angular accelerometers. By merging two advanced technologies of micro-machined gyroscope Shkel and Howe (2002) and cochlear implants S.U. Ay, F.-G. Zeng, and Shen (1997), it is possible to build a micro-vestibular neural prosthetics which restores balance function, consumes little power, and can be made in batches.

The approach reported in this paper is based on a custom design of sensors using the MEMS technology and a custom analog-digital design of the pulse generating unit converting rotational information into electrical stimulus, Figure 2(b). The proposed design can potentially integrate sensors alongside with control electronics on the same silicon chip in a volume smaller than 1 cubic centimeter. Such "balance on-a-chip" system might potentially replace the function of the damaged vestibular end-organ by providing 3-dimensional motion information for people who have permanently lost peripheral vestibular function.

2. VESTIBULAR SYSTEM AND FUNCTION

The properly functioning vestibular system is responsible for a number of reflexes and reactions critical for achieving and maintaining equilibrium of the body and stabilization of images on the retina as the head and body are moved. The vestibular system comprises the non-acoustic portion of the inner ear and consists of three semicircular canals and two otolith structures called the utricle and the saccule. The sense organs of the semicircular canals detect rotational head movements, while the sense organs of the saccule and utricle detect linear movements of the head. All of these organs have small sensory hair cells that send pulses through the nerves to the brain, where information about head movement is combined with information from the eyes, muscles, and joints, which are then interpreted.

Angular accelerations stimulate the semicircular canals. The semicircular canals are three approximately circular canals whose planes are mutually orthogonal. Each canal is filled with fluid, endolymph, which, by virtue of its inertia, flows through the canal whenever an angular acceleration in the plane of the canal is experienced by the head. Flow of the endolymph deflects the cupula, a flapper-like valve which seals an expanded portion of each duct called the ampulla. Displaced endolymph Bends the tiny hairs of sensory cells inside the canals and chambers, initiating nerve impulses that pass along the vestibular nerve to the brain. The impulses provide information to the brain about changes in head position.

3. SYSTEM DESIGN

The purpose of the semicircular canal prosthesis is to restore balance function. Ideally, the prosthesis will be able to sense motion with sufficient precision and to deliver signal to the central neural system matching signal that the natural organ would generate, thus mimicking the dynamic vestibular function, Figure 2(a). The device includes three main functional units - a sensing unit, a pulse generator, and a stimulator, Figure 2.

Figure 2(b) presents the functional blocks of the circuit components of a vestibular implant. The electronics include a sensing unit, a pulse generating unit, and a current stimulator Liu et al. (2003). The sensing unit includes a gyroscope, a low-pass filter and a differentiator; it detects the motion of the head and sends out the analog voltage signal proportional to angular acceleration about the sensing axis. The pulse generator consists of a transfer function unit and a voltage-to-frequency converter; it generates monophasic voltage pulses based on a selected mathematical

model describing biomechanics of the vestibular organ. The current source includes monophasic-to-biphasic converter (Smith triggers and analog switches) and a current mirror; they convert the monophasic voltage pulses to biphasic, charge-balanced, cathodic-first current pulses which can be used to stimulate vestibular neurons.

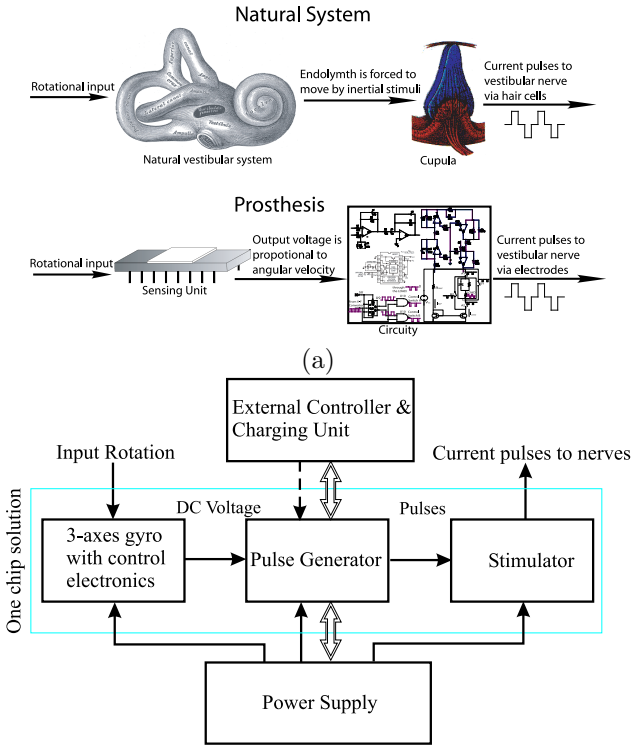

Fig. 2. (a) MEMS-based neural vestibular prosthesis is mimicking functionality of the natural vestibular end-organ; (b) Functional block-diagram of the vestibular prosthesis

3.1 Sensing Unit

The discussed unilateral prosthesis is utilizing a custom made single-axis Micro-Electro-Mechanical System (MEMS) gyroscope, developed by UCI Microsystems Laboratory mic, Figure 3(a). Using MEMS technology, big and expensive mechanical devices can now be realized as micron-size structures integrated on one chip, together with electronics, Shkel (2001). The gyroscope prototypes used in these experiments were packaged together with preamplifiers in the same package by direct wire bonding Figure 3(b). The gyroscope is approximately $2\times2mm^2$ in size with a minimum features $5\mu m$.

Our micromachined gyroscopes use vibrating element to measure rotational velocity based on the Coriolis principle A. Shkel, C.Acar, and Painter (2005).

In the basis of operation, the proof-mass, which constitute the active portion of the sensor, is

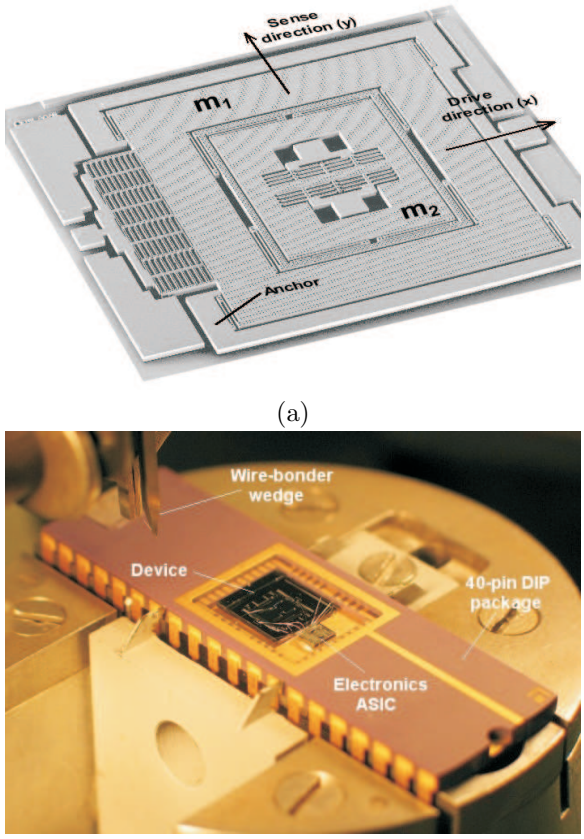

Fig. 3. (a) Scanning Electron Micrograph (SEM) of a prototype bulk-micromachined gyroscope Acar (2004); (b) A prototype gyroscope packaged together with preamplifiers in the same package by direct wire bonding

driven by an oscillator circuit at a precise amplitude X_D and high frequency ω_n, $x(t) = X_D sin(\omega_n t)$. When subjected to a rotation with angular velocity Ω, the proof-mass will be subjected to the Coriolis force. The resultant Coriolis force is perpendicular to both the input rate and the instantaneous radial velocity in the drive direction. This produces a motion of the proof-mass, $y(t)$ in direction perpendicular to its initial oscillation:

$$\|y(t)\| = \frac{2X_D\Omega Q}{\omega_n} \tag{1}$$

This expression shows that the output sense deflection is proportional to the input angular velocity. The gyroscope response is also directly proportional to quality factor Q of the device. To improve performance of micromachined gyroscopes, the devices have to be vacuum packaged to achieve high amplitude of response in the sense direction. Detection of the Coriolis response is extremely challenging, since it requires measurement of picometer-scale oscillations in the sense mode, while the proof-mass oscillates with tens of microns amplitude in the drive mode. Synchronous demodulation technique is commonly used

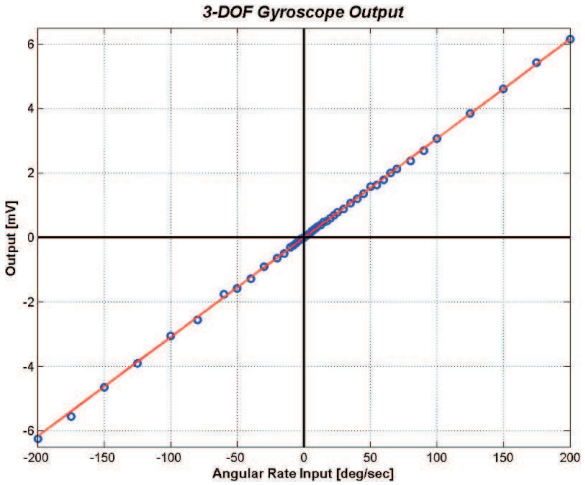

(a)

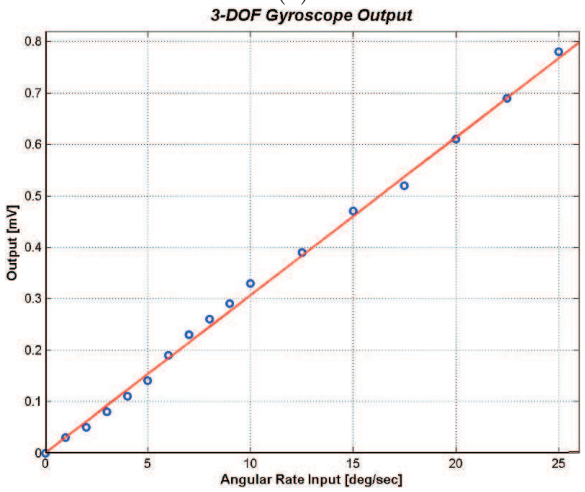

(b)

Fig. 4. The angular rate input vs. voltage output plot obtained from the 3-DOF gyroscope with 2-DOF sense mode (a) in the range -200^0/sec to -200^0/sec; (b) in the range 0^0/sec to 25^0/sec

to tackle this problem. A high-frequency carrier signal is imposed on the structure. An array of differential capacitors is used to detect pico-meter scale deflections due to the Coriolis induced motion. The difference of the outputs of the differential amplifiers is amplitude demodulated at the career signal frequency, yielding the Coriolis response signal at the driving frequency.

Using the synchronous demodulation technique, a sensitivity of $0.0694mV/^0/sec$ and a noise floor of $0.211mV/\sqrt{Hz}$ at 50 Hz bandwidth was measured. This yields a measured resolution of $3.05^0/sec/\sqrt{Hz}$ at 50 Hz bandwidth, Figure 4

The gyroscope is sensing any type of angular rotation (constant or non-constant rotational rate), while the natural vestibular organ is only responding to the angular acceleration. Thus, in order to mimic the natural organ, the supporting circuit differentiates the output voltage of the gyroscopes to produce the signal proportional to the angular

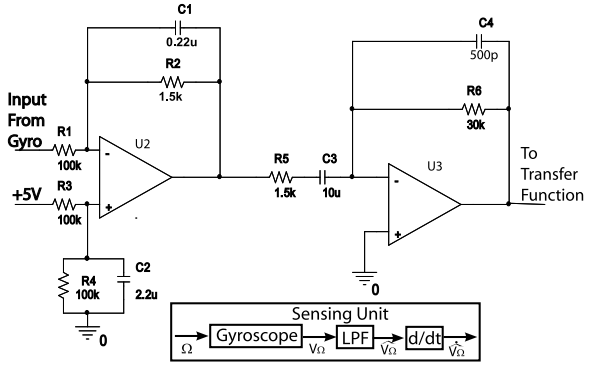

Fig. 5. Sensing Unit includes a gyroscope and low-pass filter and differentiator

acceleration. In our implementation, the circuit is utilizing a low-pass filter before the differentiator for minimizing the effect of high-frequency noise, Figure 5.

3.2 Pulse Generator

The gyroscope detects the motion of the head and sends the analog voltage signal to a pulse generator. The pulse generator consists of a transfer function unit emulating dynamics of the natural vestibular organ, Figure 6. It uses a fifth order transfer function to convert input angular acceleration to the frequency shift from the rest firing rate of the vestibular neurons. The unit than uses a Voltage-to-Frequency converter to provide a more physically relevant output.

The transfer function emulating dynamics of the natural vestibular organ is modeled as a linear torsion-pendulum system Steinhausen (1931); von A. A. Egmond et al. (1949). In this model, the cupula and endolymph are treated as a heavily damped, second-order linear system, where the cupula angular deflection $\varepsilon(t)$ is related to angular acceleration $\alpha(t)$ by differential equation Steinhausen (1931); von A. A. Egmond et al. (1949)

$$\Theta\frac{d^2\varepsilon(t)}{dt^2} + \Pi\frac{d\varepsilon(t)}{dt} + \Delta\varepsilon(t) = \Theta\alpha(t) \qquad (2)$$

with $\tau_1 = \Pi/\Delta$ and $\tau_2 = \Theta/\Pi$ are two time constants defined by morphology and material properties of the end-organ. A more complex linear model defining the relationship between the input angular acceleration and overall change in firing rate of neurons is described by

$$H(s) = \frac{\tau_A s}{1+\tau_A s}\cdot\frac{1+\tau_L s}{(1+\tau_1 s)(1+\tau_2 s)}, \qquad (3)$$

where τ_1 and τ_2 and two time constant of the pendulum model described above, τ_A is related to the level of neuron adaptability, and τ_L is the

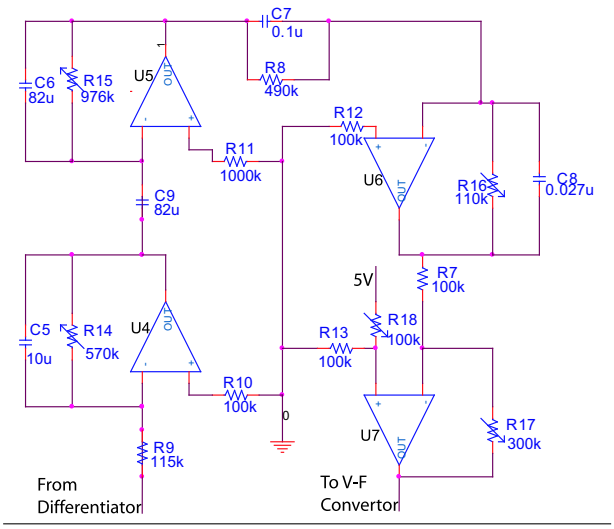

Fig. 6. Transfer function mimicing dynamics of the semicircular canals of the squirrel monkey model(reported in Goldberg and Fernandez (1971))

dynamical-electrical time constants Goldberg and Fernandez (1971).

Experimentally obtained results in Goldberg and Fernandez (1971) for the squirrel monkey model estimate $\tau_1 = 5.7sec$, $\tau_2 = 0.003sec$, $\tau_A = 80sec$, and $\tau_L = 0.049sec$. We use these experimentally defined time-constants for the design of equivalent circuit, Figure 6.

Four operational amplifiers are used to implement the transfer function relating the input angular acceleration and the frequency shift form the rest firing rate of the vestibular neurons (the firing rate when there is no rotational stimulus). The transfer function is separated in three parts: $H(s) = H_1(s) \cdot H_2(s) \cdot H_3(s)$, where

$$H_1(s) = K_1 \frac{1}{1+\tau_1 s} = -\frac{R_{14}}{R_9 \cdot (1 + R_{14} \cdot C_5 \cdot s)}$$
$$H_2(s) = K_2 \frac{\tau_A s}{1+\tau_A s} = -\frac{R_{15} \cdot C_9 \cdot s}{1 + R_{15} \cdot C_6 \cdot s}$$
$$H_3(s) = K_3 \frac{1+\tau_L s}{1+\tau_2 s} = -\frac{R_{16} \cdot (1 + R_8 \cdot C_7 \cdot s)}{R_8 \cdot (1 + R_{16} \cdot C_8 \cdot s)}$$

K_1, K_2, K_3 are adjustable gain constants. The components of the transfer function H_1, H_2, and H_3 are defined by the operational amplifiers, U_4, U_5, and U_6 in Figure 6, respectively. The transfer function produces voltages proportional to the shift from the rest firing rate of vestibular neurons Goldberg and Fernandez (1971). An additional operational amplifier U_7 is used after the transfer function $H(s)$ to adjust the voltage corresponding to the rest firing rate. For our particular implementation, we used

$$U_{7out} = -\frac{R_{17}}{R_7} \cdot U_{7in} + \frac{R_{13} \cdot (R_7 + R_{17})}{R_7 \cdot (R_{13} + R_{18})} \cdot 5(Volt)$$

with the values of the active components defined in Figure 6. In this implementation, U_{7in} is proportional to displacement from rest firing rate and U_{7out} is proportional to firing rate. If there is no rotational stimulus, U_{7in} is equal to zero, then the scaled zero shift voltage U_{7out} becomes 2 Volt.

A Voltage-to-Frequency (V-F) converter (AD537) is used to convert the voltage signals corresponding to the shift from the rest firing rate to the equivalent frequency pulses. The corresponding input/output relationship is Analog Devices (2000)

$$F_0 = \frac{V_{IN}}{10 R_{19} C_{10}} \tag{4}$$

In our implementation we choose $R_{19} = 10k\Omega$ and $C_{10} = 0.1\mu F$ resulting in $F_0 = 100 \cdot V_{IN}(Hz)$. The output is binary - 0 Volt (OFF) and 5 Volt (ON), and the duty time is 50%. For the selected parameters, the static F_0 is $100(Hz/Volt) \times 2(Volt) = 200Hz$.

3.3 Current Source

The current pulses sent via neurons to brain are delivered by ion flow, so that the total charge sent to the nerve should be zero. Since tissue impedance is changing over time, a voltage source may not maintain constant current for charge delivery. Thus, a stimulation with current source, instead of a voltage source, is required to transmit signals via neurons. The overall charge sent via neural fibers should be zero (e.g., S.U. Ay, F.-G. Zeng, and Shen (1997)), so that the integration of the current over time is zero. If this condition is not satisfied, the neuron could be destroyed. In order to satisfy these constrains, monophasic voltage signal has to be changed to biphasic current signal.

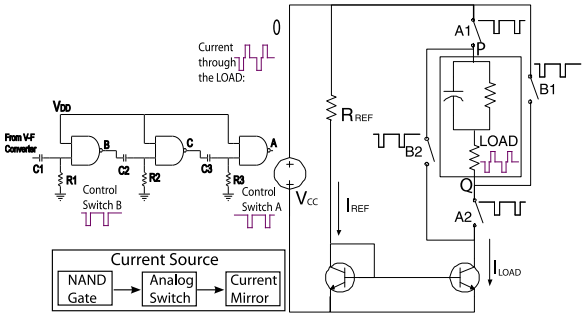

Fig. 7. Current source converting monophasic voltage pulses to biphasic current pulses

Figure 7 shows our conceptual implementation of the current source, which includes a current mirror, analog switches and Smith triggers. The analog switches and Smith triggers convert monophasic signal to biphasic signal, and the current mir-

ror provides current output that is not affected by the load impedance.

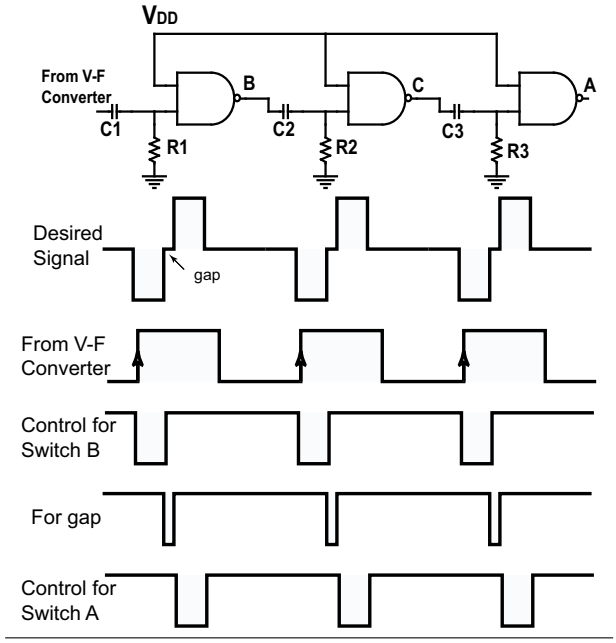

Fig. 8. Control signal of the switches using Smith triggers

For each NAND Gates, Figure 8, when one of the input is kept high, another input (V_1) governs the output. As soon as the voltage at V_1 falls below V_{T-} (1.8Volt), V_{OUT} changes from low to high. So the pulse duration (PD) in V_{OUT} can be calculated by

$$e^{\frac{PD}{\tau}} = \frac{V_{DD}}{V_1} \tag{5}$$

The maximum neuron firing rate is around 250Hz Gong and Merfield (2002), so the minimum duration for each firing cycle is around 4ms. Since the pulse duration in V_{OUT} should be less than half of the firing cycle, the PD+ and PD- are designed to be 1ms. Substituting 5 Volt in V_{DD} and 1.8 Volt in V_{T-}, time constant τ can be calculated from Equation (5)

$$\tau = \frac{PD}{ln(\frac{V_{DD}}{V_1})} = \frac{PD}{ln(\frac{5}{1.8})} = 1.0217$$

Three Smith triggers are used in our implementation to achieve control signal for the switches.

The electrical properties of a biological tissue can be modeled by an equivalent circuit as a resistor and a capacitor in parallel, plus a resistor in series. The values of the resistors and capacitor in this model are fluctuating. By using the current mirror illustrated in Figure 7, the voltage across the LOAD may change due to changes in impedance of the tissue, however the current through the LOAD will not be affected.

4. EXPERIMENTAL RESULTS

Based on the discussed design, a circuitry prototype is implemented on a Printed Circuit Board (PCB), Figure 9. It consists of a sensing unit which includes a z-axis gyroscope, a low-pass filter and a differentiator; a pulse generating unit which includes a transfer function unit and a voltage-to-frequency converter, and a current source which includes Smith triggers, analog switches and a current mirror. Two nine volt batteries are used as a power supply for the prototype circuitry and the sensor. Nine potentiometers are utilized to adjust for the resistance parameters, including four time constants in the transfer function (τ_A, τ_1, τ_2, and τ_L), rest firing rate, gain of the transfer function, positive and negative pulse duration, and magnitude of the current pulse.

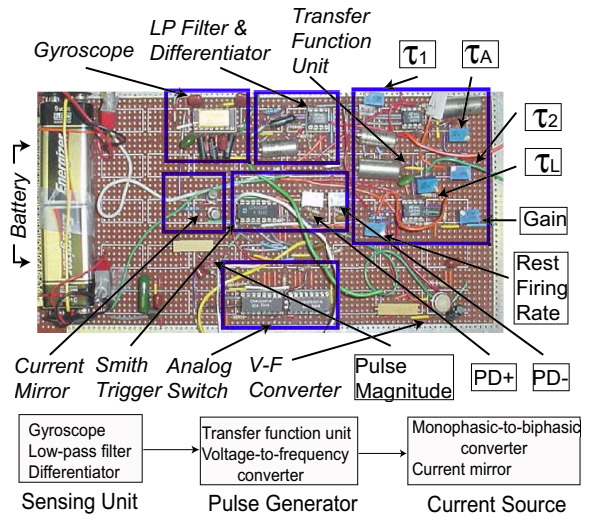

Fig. 9. Printed Circuit Board (PCB) prototype of the electrostimulatory unilateral prosthesis

4.1 Time Domain Response

A fragment of the circuit response to sinusoidal voltage input is illustrated in Figure 10 at three different time scales (500ms, 50ms, 2ms in (a), (b), (c), correspondingly). The voltage response is recorded using Virtual Bench 2.1.1 (a Labview program by National Instruments) through a data acquisition board (National Instruments BNC-2110). Then the data was saved as the text file, which was subsequently imported and analyzed in Matlab.

Legend (1) in Figure 10 is generated from a signal generator at 2Hz frequency, 0.5V peak amplitude, and 2.43Volt offset, and it acts as the output from the gyroscope. The gyro calibration shows that the corresponding motion is harmonic rotation with zero offset, 2Hz frequency and 40degree/second peak amplitude. Legend (2) shows

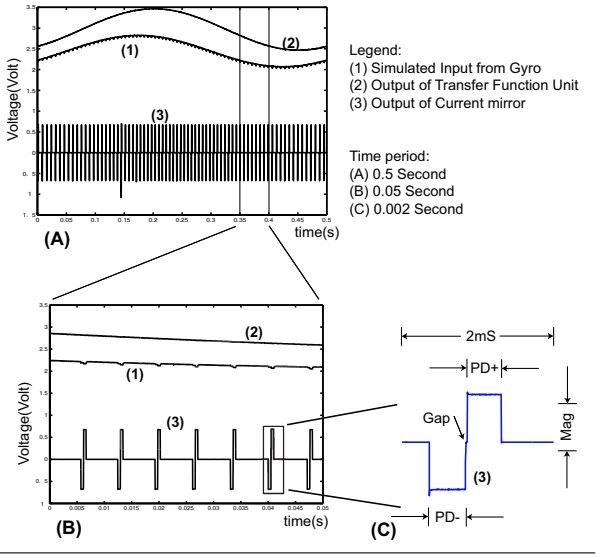

Fig. 10. Circuitry response to harmonic inertial stimuli

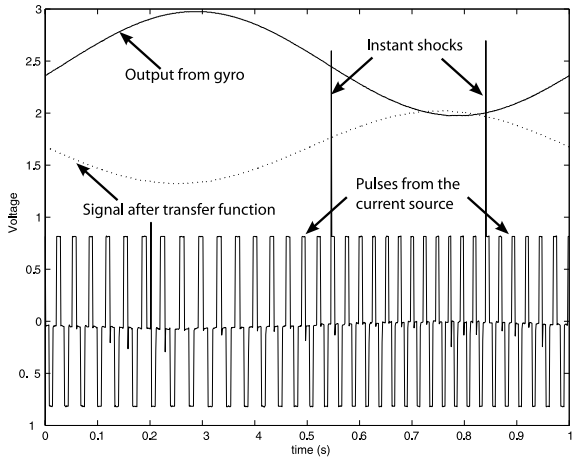

Fig. 11. Response of the prosthesis to the harmonic inertial excitation

the voltage signal after the transfer function unit, and it is proportional to the pulse rate of legend (3), Figure 10 (a). For the convenience of recording, voltage across the load (Legend 3) is measured. The current through the load is obtained by dividing the voltage by the load impedance, which in turns consists of biphasic, charge-balanced, and cathode-first pulses. Changing the load impedance, the amplitude of voltage pulses changes, and the amplitude of the current pulses is kept constant. Figure 10 (b) and (c) scale the time duration down to 50ms and 2ms, correspondingly. Figure 10 (c) illustrates the voltage pulses across the load. Three parameters of the pulse shape can be adjusted for the best performance of the stimulator, i.e., positive and negative pulse duration (PD+, PD-) and pulse magnitude (Mag).

4.2 Response of the Prosthesis

Performance of the unilateral vestibular prosthesis was compared to the experimentally obtained results in Goldberg and Fernandez (1971) on a squirrel monkey animal model. In the experiment the animal was mounted in a structure, so that the center of the head was coincident with the axis of rotation and the horizontal canal is in horizontal plane. Sinusoidal rotations with frequency $0.1 - 8Hz$ were sequentially applied and response of neurons firing in the vestibular nerve were monitored and recorded. In our experiment, we initially placed our prototype on a rate table and applied a constant rotational input. This allowed us to build the input/output relations for the gyroscope. After that we modeled the response of the gyroscope under the same rotational conditions as those reported in Goldberg and Fernandez (1971). A fragment of the prosthesis response to inertial stimulus is illustrated in Figure 11

The continuous line in Figure 11 is a sinusoidal input rotation of the rate table as it were measured by the sensing unit (gyroscope) of the prosthesis. The dashed line is the analog signal after the input from the gyroscope was fed through the transfer function of the pulse generating unit. The fixed amplitude pulses are supperimposed in the same figure to illustrate dependence and similarity of the signal provided to the vestibular nerve by the natural vestibular system and the developed vestibular prosthesis. For the illustration purposes the input rotation was harmonic with the frequency $1Hz$ and with the acceleration amplitude $250^0/sec^2$. The output biphasic current pulses generated by the prosthesis are $40spikes/sec$ for the resting firing rate and with maximum at $50spikes/sec$ and minimum at $30spikes/sec$. Note that the resting firing rate and sensitivity can be easily scaled using the amplifier U_7. Instant shocks in Figure 11 can be attributed to conversion of the digital signal to analog signal. Such short-term shocks are unavoidable and can be minimized by adding a small capacitor parallel to the load.

In Figure 12 we provide a side-by-side comparison between the experimental results on squirrel monkey Goldberg and Fernandez (1971) and the design vestibular prosthesis. Data points marked with(X) represent experimentally measured responses in firing of nerves in semicircular canals of the squirrel monkey animal model Goldberg and Fernandez (1971). The comparison is performed for the harmonic angular acceleration with frequencies between 0.1 Hz and 8 Hz. The gain results demonstrate a very close match between two experiments, however there is a slight phase shift between the data obtained from the prosthesis and the animal experiment. This miss-matching is negligible at low frequencies and it gradually increasing at higher frequencies. We believe higher order mathematical models of the biomechanics of

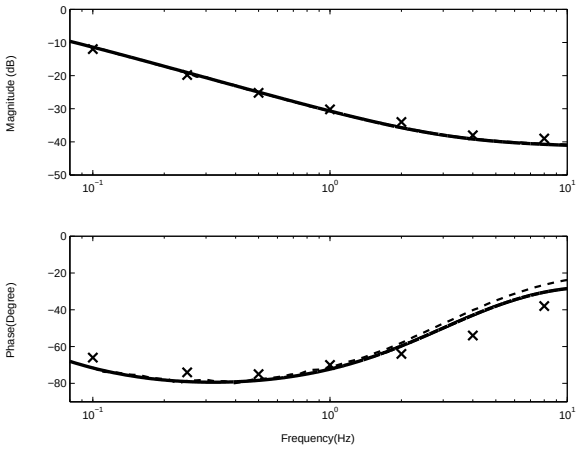

Fig. 12. Comparison of response of the circuitry and of the natural vestibular system in the squirrel monkey experiments reported in the literature Goldberg and Fernandez (1971)

the vestibular organ are required to capture this phenomena.

5. REMAINING ISSUES AND FUTURE DIRECTIONS

This paper discusses initial implementation and experimental verification of the prototype of the electronic prosthesis mimicking the function of a unilateral semicircular canal. Our preliminary results demonstrated a possibility of designing a MEMS electronic system which can closely match the response of the natural vestibular organ in the presence of unilateral rotation.

Our next step is to demonstrate on live animal models a possibility for sensory substitution. We believe, damaged, or temporarily disabled, vestibular organ can be effectively replaced by the electrostimulatory prosthesis with the proposed architecture.

Even though some preliminary results already available in the literature, we will expect a lot of future activities in trying to understand the issues of the most effective stimulation of the vestibular nerve and achieving vestibular selectivity of the stimulation.

6. ACKNOWLEDGMENT

Author would like to acknowledge Dr. Acar for contribution in development of MEMS gyroscope, J. Liu for work on implementation of Pulse Generator and Current Source, and Dr. F-G. Zeng for useful discussions on electrical stimulation.

This project was partially supported by NSF CAREER award CMS-0449442.

REFERENCES

http://mems.eng.uci.edu. UCI Microsystems Laboratory.

A. Shkel, C.Acar, and C. Painter. Two types of micromachined vibratory gyroscopes. *Int. IEEE Sensors Conference*, October 2005. Irvine, CA, USA.

Cenk Acar. *"Robust Micromachined Vibratory Gyroscopes"*. Ph.D. thesis, Dept. of MAE, University of California - Irvine, 2004.

Inc. Analog Devices. Ad537 reference data sheet, 2000. URL `http://www.analog.com`.

J. M. Goldberg and C. Fernandez. Physilology of peripheral neurons innervating semicircular canals of the squirrel monkey. II. Response to sinusoidal stimulation and dynamics of peripheral vestibular system. *J. Neurophysiol.*, 34: 661–675, 1971.

W. Gong and D.M. Merfield. System design and performance of a unilateral horizontal semicircular canal prosthesis. 49:175–181, February 2002.

J. Liu, A. M. Shkel, K. Nie, and F.G. Zeng. Circuit with adjustable parameters mimicking function of the national vestibular end-organ. In *Proc. of the 1st International IEEE EMBS Conference on Neural Engineering*, Capri Island, Italy, March 2003.

A. Shkel. Micromachined gyroscopes: Challenges, design solutions, and opportunities. *2001 SPIE Annual International Symposium on Smart Structures and Materials*, 2001. (Invited Paper) March, 2001, Newport Beach, CA.

A. M. Shkel and R. T. Howe. Micro-machined angle-measuring gyroscope, November 2002.

W. Steinhausen. ber den nachweis der bewegung der cupula in der intakten bogengangsampulle des labyrinthes bei natrlichen rotatorischen und calorischen reizung. *Arch. Ges. Physiol.*, 228: 322–328, 1931.

S.U. Ay, F.-G. Zeng, and B.J. Shen. Hearing with Bionic Ears. *IEEE Circuits and devices*, 5:18–23, 1997.

von A. A. Egmond, J.J. Groen, and L.B.W.Jongkees. The mechanics of the semicircular canal. *J. Physiol., London*, 110: 1–17, 1949.